

Article

Novel Multicomponent Titanate-Germanate Glasses: Synthesis, Structure, Properties, Transition Metal, and Rare Earth Doping

Wojciech A. Pisarski ^{1,*}, Karolina Kowalska ¹, Marta Kuwik ¹, Justyna Polak ¹, Ewa Pietrasik ¹, Tomasz Goryczka ² and Joanna Pisarska ¹

¹ Institute of Chemistry, University of Silesia, Szkolna 9 Street, 40-007 Katowice, Poland; k.kowalska119@gmail.com (K.K.); marta.kuwik88@gmail.com (M.K.); justyna.polak@us.edu.pl (J.P.); ewa.pietrasik@us.edu.pl (E.P.); joanna.pisarska@us.edu.pl (J.P.)

² Institute of Materials Science, University of Silesia, 75 Pułku Piechoty 1A Street, 41-500 Chorzów, Poland; tomasz.goryczka@us.edu.pl

* Correspondence: wojciech.pisarski@us.edu.pl

Received: 13 August 2020; Accepted: 29 September 2020; Published: 4 October 2020



Abstract: Novel multicomponent titanate-germanate glasses singly doped with transition metal (Cr^{3+}) and rare earth ions (Eu^{3+}) were synthesized and the glass transition temperatures and thermal stability parameters were determined using DSC measurements. X-ray diffraction analysis confirmed fully amorphous nature of the received samples. Their structural and optical properties were compared with germanate glasses without TiO_2 . Correlation between local structure and optical properties in titanate-germanate glasses is well evidenced by FT-IR, Raman, EPR, and luminescence spectroscopy. In particular, luminescence spectra and their decays are examined for glass samples, where GeO_2 was partially substituted by TiO_2 .

Keywords: glasses; structure-property relationship; Cr^{3+} ; Eu^{3+} ; spectroscopic parameters

1. Introduction

Since 1986 the formation of TiO_2 containing glasses has been investigated in detail [1–8]. Unfortunately, most of titanate glass systems are partly crystallized. The obtained systems possess crystalline phases mainly because of different titanates and their thermal stability parameters are relatively low, which makes them unsuitable for optical-fiber applications. In fact, it is difficult to prepare thermally stable and fully amorphous systems with relatively high titanium oxide content. On the other hand, germanate glasses have quite strong chemical and mechanical stability useful for optical fiber drawing and belong to low-phonon glass family. Compared to other low-phonon glass systems such as tellurite glasses, germanate based glass-host matrices have relatively large glass-forming region. In particular, thermal stability parameter referred to as a difference between crystallization onset T_x and glass transition temperature T_g is considerably higher for germanate-based glass with $\Delta T = 155\text{ }^\circ\text{C}$ [9] than tellurite based glass with $\Delta T = 27\text{ }^\circ\text{C}$ [10]. Quantum efficiencies for ${}^4\text{F}_{3/2} \rightarrow {}^4\text{I}_{11/2}$ (Nd^{3+}) and ${}^4\text{I}_{13/2} \rightarrow {}^4\text{I}_{15/2}$ (Er^{3+}) transitions of rare earth ions in germanate glasses based on $\text{GeO}_2\text{-BaO-Ga}_2\text{O}_3$ are close to 80% [11] and 71% [12], respectively. Their values are also larger compared to main near-infrared laser transitions of Nd^{3+} ($\eta = 68\%$) and Er^{3+} ($\eta = 46\%$) ions in glasses based on $\text{TeO}_2\text{-ZnO}$ [13,14]. Various glass-modifiers were tested in order to obtain thermally stable and amorphous systems with excellent luminescence properties. Systematic studies clearly indicate that the effect of modifier oxides on emission properties of rare earth ions in different glass matrices is significant [15]. Influence of modifier oxides M_2O where M denotes Li, Na, K, Rb, Cs [16], MO where M = Ca, Sr, Ba [17,18], M_2O_3 where M = Al or Ga [19] and MO_2 where M = Te, Ge, Si [20] on local

structure of glasses and their multifunctional properties and potential applications has been presented and discussed. Special attention has been paid to germanate glasses with different glass-modifiers. High niobium oxide content in alkali germanate glasses was evidenced by the optical absorption, DSC and XRD analysis, FT-IR, and Raman spectroscopy. Marcondes et al. [21] suggest that high niobium oxide content causes an increase in the glass-host network and strongly modifies thermal, structural, and optical properties of alkali germanate glasses. These structural and optical aspects for Eu^{3+} doped germanate glasses modified by MO/MF_2 where M denotes Ca, Sr, Ba, have been also studied [22]. In particular, the influence of the oxide and fluoride glass-modifiers on local structure of germanate glasses has been examined using X-ray diffraction analysis. The experimental results clearly demonstrate that samples with modifiers MO/MF_2 (M = Ca or Sr) are crystalline, whereas samples with BaO and/or BaF_2 are fully amorphous. Further studies revealed that modification of germanate glasses by P_2O_5 allows control of their local structure and visible luminescence. The increase of P_2O_5 content leads to the reduction of spectral linewidth and the shift of emission band of Eu^{3+} ions in germanate glass to shorter wavelengths [23]. The effect of the spectroscopic properties of Tm^{3+} ions for different compositions with varying $\text{Nb}_2\text{O}_5/\text{La}_2\text{O}_3$ ratios has been studied and the optical concentration of glass components for efficient 1.8 μm near-infrared laser applications was determined [24]. Rare earth-doped germanate glasses modified by Bi_2O_3 [25], Y_2O_3 and Nb_2O_5 [26] have been also analyzed for mid-infrared emission. These aspects were not yet examined for germanate-based glass in the presence of titanium dioxide.

In the present work, multicomponent glasses based on $\text{TiO}_2\text{-GeO}_2\text{-BaO-Ga}_2\text{O}_3\text{-M}_2\text{O}_3$ (M—rare earth or transition metal) were successfully synthesized using conventional high-temperature melting and their structure and properties are presented and compared to the glasses in the absence of TiO_2 . Local structure and properties of multicomponent glasses containing two glass-network formers GeO_2 and TiO_2 were characterized using various experimental techniques: X-ray diffraction (XRD), differential scanning calorimetry (DSC), electron paramagnetic resonance (EPR), Raman and Fourier-transform infrared spectroscopy (FT-IR), absorption and luminescence spectroscopy. Transition metal (Cr^{3+}) and rare earth (Eu^{3+}), commonly known as spectroscopic probe, were used as the optical dopants. Our new preliminary results for titanate-germanate glasses are presented and discussed in relation to potential visible (Eu^{3+}) and near-infrared (Cr^{3+}) luminescence applications. In particular, luminescence spectra and decay curves were examined for glass samples, where germanium dioxide was substituted by titanium dioxide and the relative molar ratio of these two main glass-former components is equal to $\text{GeO}_2:\text{TiO}_2 = 1:1$. In previous work TiO_2 was substituted by GeO_2 in multicomponent germanoniobophosphate glass system allowing the glass stabilization against devitrification and the improvement of photoluminescence behavior, but amount of titanium dioxide playing the role as glass-network modifier did not exceed 15 molar % [27].

2. Materials and Methods

Multicomponent glasses undoped and doped with transition metal or rare earth were prepared: $30\text{TiO}_2\text{-}30\text{GeO}_2\text{-}30\text{BaO-}10\text{Ga}_2\text{O}_3$ (referred as TiGe), $30\text{TiO}_2\text{-}30\text{GeO}_2\text{-}30\text{BaO-}9.75\text{Ga}_2\text{O}_3\text{-}0.25\text{Cr}_2\text{O}_3$ (TiGe-Cr), $30\text{TiO}_2\text{-}30\text{GeO}_2\text{-}30\text{BaO-}9.75\text{Ga}_2\text{O}_3\text{-}0.5\text{Eu}_2\text{O}_3$ (TiGe-Eu) and their structure and properties were compared to glass samples without titanium dioxide $60\text{GeO}_2\text{-}30\text{BaO-}10\text{Ga}_2\text{O}_3$ (referred as Ge), $60\text{GeO}_2\text{-}30\text{BaO-}9.75\text{Ga}_2\text{O}_3\text{-}0.25\text{Cr}_2\text{O}_3$ (Ge-Cr), and $60\text{GeO}_2\text{-}30\text{BaO-}9.75\text{Ga}_2\text{O}_3\text{-}0.5\text{Eu}_2\text{O}_3$ (Ge-Eu). The concentrations of components are given in molar %. Titanate-germanate glasses were synthesized using high-temperature melt quenching-technique. The appropriate amounts of glass components (metal oxides of high purity 99.99%, Aldrich Chemical Co., St. Louis, MO, USA) were mixed and melted (1200 °C/0.45 h).

The amorphous nature of samples was confirmed by X-ray diffraction measurements (X'Pert Pro diffractometer, Panalytical, Almelo, The Netherlands) with Cu $\text{K}\alpha_1$ radiation ($\lambda = 1.54056 \text{ \AA}$). The Cu X-ray tube operating at 40 kW/30 mA was used. Diffraction patterns were measured in step-scan mode with a step size of 0.05° and time per step of 10 s. The glass samples were characterized

by a SETARAM Labsys thermal analyzer (SETARAM Instrumentation, Caluire, France) using the DSC method. The DSC curves were acquired with heating rate of 10 °C /min.

The electron paramagnetic resonance spectra were performed using Bruker EMX EPR spectrometer (Bruker-Biospin, Karlsruhe, Germany) working at X-band frequency (9.8 GHz). The EPR instrument parameters are as follows: central field 3480 G, modulation amplitude 2.0 G, time constant 40.96, gain 1×10^4 G, and microwave power 20.12 mW. The infrared spectra using the ATR technique were recorded over the frequency range of 1000–350 cm^{-1} using a Nicolet™ iS™ 50 FT-IR spectrometer (Thermo Fisher Scientific, Waltham, MA, USA) with a diamond attenuated total reflectance (ATR) module. The Raman spectra using a Thermo Fisher Scientific™ DXR™2xi Raman Imaging Microscope and laser working as the source (24 mW power) with excitation wavelength 780 nm were measured. The laser was directly focused on the glass sample with an Olympus long-working-distance microscope objective (50×).

Next, the glass samples were characterized using absorption (Varian Cary 5000 UV-VIS-NIR spectrophotometer, Agilent Technology, Santa Clara, CA, USA) and luminescence spectroscopy (laser equipment, which consists of PTI QuantaMaster QM40 spectrofluorometer, tunable pulsed optical parametric oscillator (OPO), Nd:YAG laser (Opotek Opolette 355 LD, Carlsbad, CA, USA), double 200 mm monochromators, multimode UVVIS PMT R928 and Hamamatsu H10330B-75 detectors (Hamamatsu, Bridgewater, NJ, USA), PTI and ASOC-10 USB-2500 oscilloscope). Resolution for spectral measurements was ± 0.1 nm, whereas decay curves with accuracy ± 0.5 μs were acquired.

3. Results and Discussion

3.1. Undoped Titanate-Germanate Glasses

Titanate-germanate glasses were successfully synthesized and their structure and properties were examined using XRD, DSC, FT-IR, and Raman spectroscopy. Figure 1 shows XRD patterns (a, b), DSC curves (c, d), FT-IR (e), and Raman (f) spectra for titanate-germanate glasses referred as TiGe. They are compared to the results obtained for glass samples without titanium dioxide (Ge).

The received glass samples (TiGe and Ge) reveal X-ray diffraction patterns characteristic for amorphous systems and narrow diffraction lines typical for crystalline materials are not observed. Moreover, any significant structural changes in the XRD patterns have been observed for glass samples after transition metal (TiGe-Cr) or rare earth (TiGe-Eu) doping. It clearly indicates that titanate-germanate glasses are able to accommodate transition metal or rare earth ions and the samples are still fully amorphous. Our previous studies for lead borate glasses demonstrated that rare earth oxides influence on the resistance to crystallization. In contrast to sample with Nd_2O_3 , several crystalline peaks due to the ErBO_3 phase are present after addition of Er_2O_3 to the base lead borate glass, suggesting the increased tendency toward crystallization [28]. From DSC curves measured for glass samples (TiGe and Ge), the glass transition temperature T_g and thermal stability parameter ($\Delta T = T_x - T_g$) were determined. In contrast to germanate glass (Ge), the additional exothermic peak representing the crystallization of the glass can be observed for glass sample with the presence of TiO_2 . It is well evidenced that the thermal stability parameter is reduced where GeO_2 is partially replaced by TiO_2 . The glass transition temperature T_g increases from 620 °C to 690 °C suggesting less open glass structure [29]. These thermal parameters T_g and ΔT are also schematized on Figure 1c. The Raman and FT-IR spectra between 350 cm^{-1} and 1000 cm^{-1} frequency region consists of two main bands centered at about 500 cm^{-1} and 800 cm^{-1} . Similar to previous reports for germanate-based glasses [30,31], the low-frequency band located from 400 cm^{-1} to 600 cm^{-1} is assigned to bending vibration involving Ge-O-Ge and Ge-O-Ga bridges, whereas the high-frequency band between 700 cm^{-1} and 900 cm^{-1} is attributed to asymmetric stretching vibrations of Ge-O-Ge bonds and symmetric stretching of Ge-O/Ga-O bonds. In general, Raman and FT-IR bands are shifted to lower frequency region in the presence of TiO_2 . Kamitsos et al. [31] observed similar effects for germanate glasses in function of Rb_2O . In the 630–700 cm^{-1} frequency region, the additional band located near 650 cm^{-1} is quite well observed

for glass sample with titanium dioxide. This band is due to the stretching vibration of Ti-O in TiO_6 unit [32].

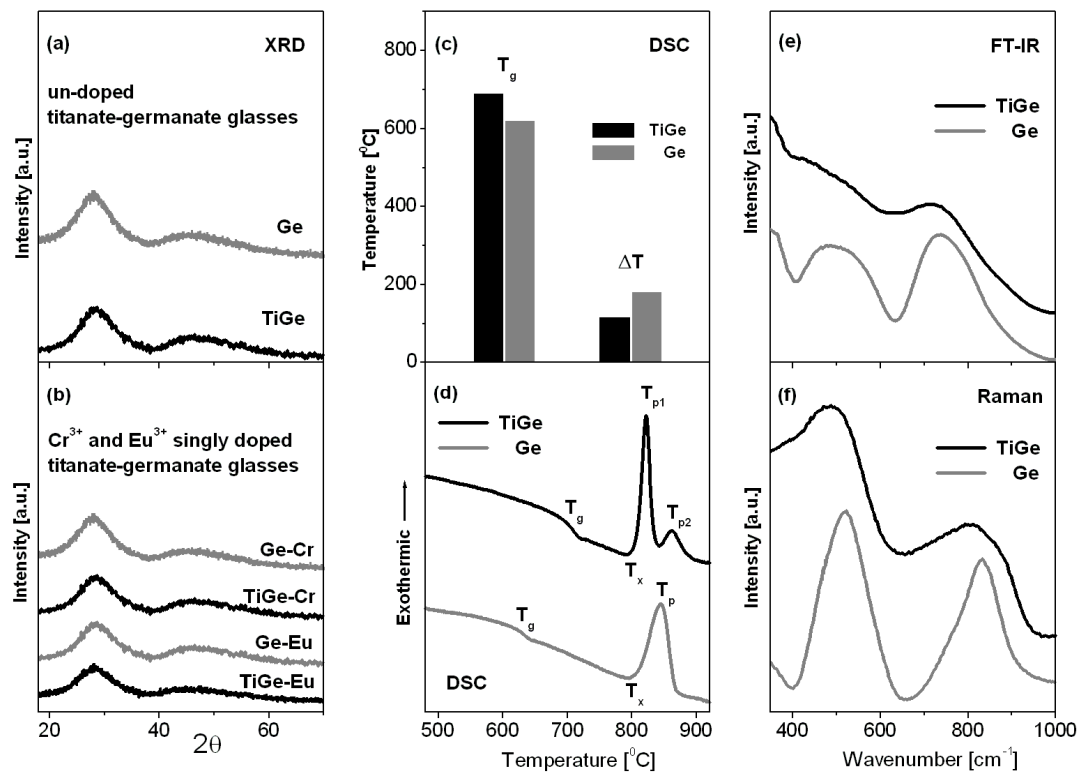


Figure 1. X-ray diffraction patterns (a,b), thermal parameters T_g and ΔT (c) and DSC curves (d), FT-IR (e) and Raman (f) spectra measured for titanate-germanate glasses (TiGe) and compared to glass samples without TiO_2 (Ge).

3.2. Titanate-Germanate Glasses Doped with Chromium Ions

Figure 2 shows results for titanate-germanate glasses doped with chromium ions, which were characterized using EPR (a), absorption (b), and luminescence (c–f) spectroscopy. Independently on samples with the presence (TiGe-Cr) or absence (Ge-Cr) of TiO_2 , the EPR spectra show two resonant signals at about $g = 4.8$ and $g = 1.97$, which evidently proves the $3+$ valence state for chromium ions and the octahedral coordination. The similar effects were observed earlier for trivalent chromium ions in lead niobium germanosilicate glasses [33] and antimony phosphate glasses [34]. These two resonance signals may be quite well interpreted. They are related to the isolated Cr^{3+} ions ($g = 4.8$) and the exchange coupled pairs $\text{Cr}^{3+}\text{-Cr}^{3+}$ ($g = 1.97$) [35]. The presence of chromium ions at trivalent state in the studied glass systems was also confirmed by the absorption spectra measurements. The spectra measured in 550–800 nm ranges show characteristic broad absorption band, which consist of three overlapped peaks due to transitions originating from 4A_2 ground state to the 4T_2 , 2T_1 , and 2E excited states of trivalent chromium, respectively. Comparing to sample Ge-Cr, the $^4A_2 \rightarrow ^2E$ transition of Cr^{3+} ions is shifted to longer wavelengths in the presence of titanium dioxide (TiGe-Cr). At this moment, it should be also noticed that the second absorption band associated to the $^4A_2 \rightarrow ^4T_1$ transition of Cr^{3+} ions is located at about 430 nm. This band has not been observed for several glasses, because it is masked by strong UV-vis absorption of the host or lies on the tail of absorption edge. However, both absorption bands of chromium ions were successfully measured by us for barium gallo-germanate glass. Thus, some important spectroscopic parameters were calculated owing to the Tanabe-Sugano diagram for d^3 electronic configuration suggesting that chromium ions in barium gallo-germanate glass are in an intermediate octahedral ligand field environment ($2.1 < Dq/B < 2.3$).

The crystal field parameters, the Racah parameters, and the related ligand field parameters are as follows: $Dq = 1557 \text{ cm}^{-1}$, $B = 732 \text{ cm}^{-1}$, $C = 2991 \text{ cm}^{-1}$, and $Dq/B = 2.13$ [36].

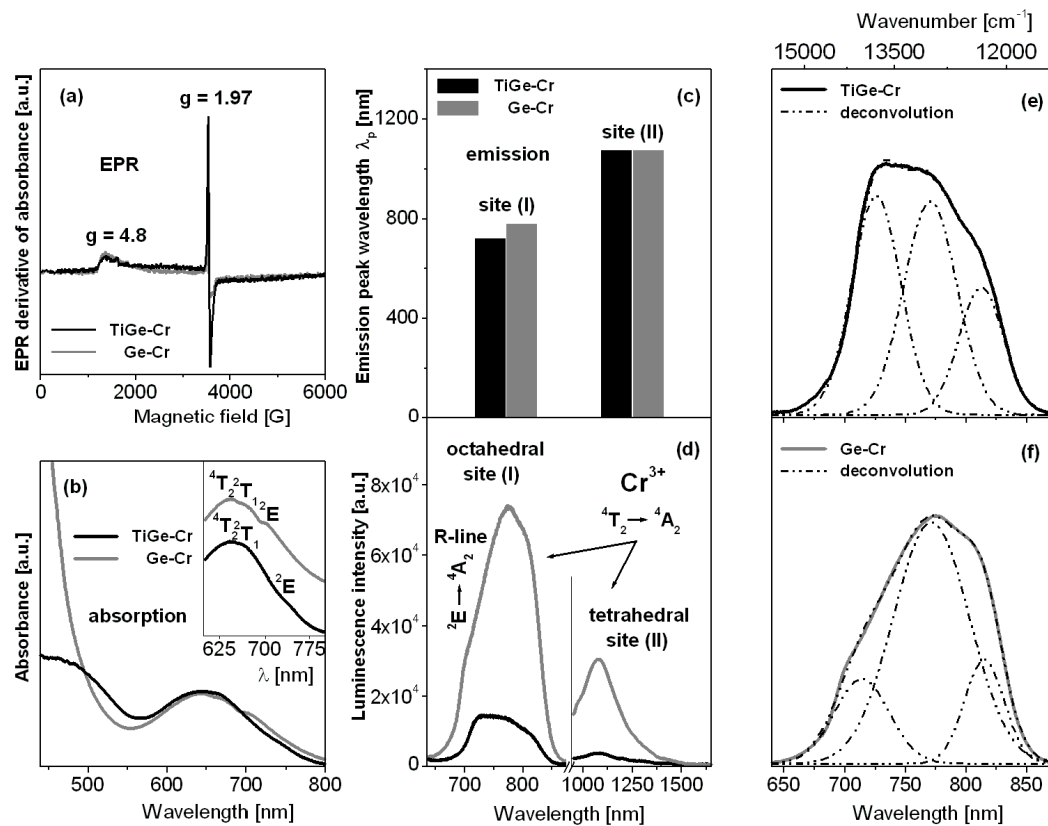


Figure 2. EPR (a), absorption (b), and luminescence (c,d) spectra measured for titanate-germanate glasses doped with chromium ions (TiGe-Cr) and compared to glass samples without TiO_2 (Ge-Cr). Deconvoluted emission bands for both glass samples TiGe-Cr (e) and Ge-Cr (f) are also given.

The near-infrared luminescence spectra of chromium ions revealed two emission bands, but both well observed lines are assigned to the transition originating from the 4T_2 excited state to the 4A_2 ground state. According to the excellent paper published recently, the near-infrared emission bands centered at about 730 nm and 1030 nm are related to the ${}^4T_2 \rightarrow {}^4A_2$ transitions in octahedral sites (I) and tetrahedral sites (II) of chromium ions [37]. Further spectroscopic analysis indicates that the intensities of luminescence bands are stronger for chromium ions located at octahedral site (I) than tetrahedral site (II). The maximum of emission peak wavelength for the ${}^4T_2 \rightarrow {}^4A_2$ transition of chromium ions in octahedral sites (I) is changed from 730 nm (Ge-Cr) to 775 nm in the presence of titanium dioxide (TiGe-Cr) in contrast to tetrahedral site (II), where both peak maxima are the same. Furthermore, the profiles of emission bands associated to transition of chromium ions in site (I) are completely different. It is especially evidenced for the ${}^2E \rightarrow {}^4A_2$ transition commonly known as R-line, which is overlapped with the ${}^4T_2 \rightarrow {}^4A_2$ transition of chromium ions in octahedral site (I). The maximum of R-line is shifted to longer wavelength from 715 nm (Ge-Cr) to 727 nm (TiGe-Cr). In order to further study the structural changes occurring in the arrangement around Cr^{3+} , the emission bands were successfully deconvoluted into three Gaussian components. The luminescence band ascribed to the ${}^4T_2 \rightarrow {}^4A_2$ transition was well divided into the red and the blue components, confirming the coexistence of two completely different site distributions for chromium ions. During the deconvolution procedure, peak wavenumber (ν), linewidth ($d\nu$), the energy gap between both 4T_2 and 2E excited states $\Delta E = E({}^2E) - E({}^4T_2)$, and the relative integrated emission line intensities $I({}^2E)/I({}^4T_2) = A_{\text{R-LINE}}/(A_{\text{RED}} + A_{\text{BLUE}})$ and $I({}^2E)/I_{\text{TOTAL}} = A_{\text{R-LINE}}/(A_{\text{RED}} + A_{\text{BLUE}} + A_{\text{R-LINE}})$ were estimated. The $A_{\text{RED}} + A_{\text{BLUE}} + A_{\text{R-LINE}}$ denotes the integrated

emission intensities of the red and the blue components of 4T_2 as well as 2E (R-line), respectively. The relative integrated intensities of the bands were measured in order to monitor the equilibrium position between the 4T_2 and 2E excited states of chromium. The results are summarized in Table 1.

Table 1. Spectroscopic parameters for chromium ions in glasses TiGe-Cr and Ge-Cr.

Spectroscopic Parameter	TiGe-Cr	Ge-Cr
$\nu_{\text{RED}} ({}^4T_2)$ (cm^{-1})	12,326	12,266
$\nu_{\text{BLUE}} ({}^4T_2)$ (cm^{-1})	12,963	12,981
$\nu_{\text{R-LINE}} ({}^2E)$ (cm^{-1})	13,755	13,986
ΔE (cm^{-1})	792	1005
$d\nu_{\text{RED}} ({}^4T_2)$ (cm^{-1})	518	480
$d\nu_{\text{BLUE}} ({}^4T_2)$ (cm^{-1})	711	900
$d\nu_{\text{R-LINE}} ({}^2E)$ (cm^{-1})	838	1082
$I({}^2E)/I({}^4T_2)$	0.63	0.21
$I({}^2E)/I_{\text{TOTAL}}$	0.39	0.17

Our calculations give interesting results. The energy gap between the 4T_2 and 2E excited states of chromium ions increases significantly from 792 cm^{-1} (TiGe-Cr) to 1005 cm^{-1} in the glass sample with the absence of titanium dioxide (Ge-Cr). The relative integrated emission line intensities denoted as A_{RED} , A_{BLUE} , and $A_{\text{R-LINE}}$ due to the ${}^4T_2 \rightarrow {}^4A_2$ and ${}^2E \rightarrow {}^4A_2$ transitions of chromium ions are also drastically changed. Thus, the relative integrated line intensity ratios of $I({}^2E)/I({}^4T_2)$ and $I({}^2E)/I_{\text{TOTAL}}$ are increased with the presence of TiO_2 in glass composition. The appropriate relative integrated line intensity ratios increase from 0.21 to 0.63 ($I({}^2E)/I({}^4T_2)$) and from 0.17 to 0.39 ($I({}^2E)/I_{\text{TOTAL}}$), when GeO_2 was partially substituted by TiO_2 , respectively. It suggests that chromium ions occupy higher crystal-field sites in germanate glasses in the presence of TiO_2 . Completely different situation was observed previously for chromium ions in lead borate glass. The energy gap between 4T_2 and 2E states was changed from 1055 cm^{-1} ($\text{PbO}:\text{B}_2\text{O}_3 = 1:1$) to 770 cm^{-1} ($\text{PbO}:\text{B}_2\text{O}_3 = 4:1$). In this case, the same Gaussian-fitting procedure was applied to evaluate spectroscopic parameters. The relative integrated line intensity ratios were nearly twice reduced, suggesting the presence of chromium ions in lower crystal-field sites with increasing PbO concentration [38].

Spectroscopic results for the studied glasses suggest that photoluminescence properties of chromium ions depend critically on titanium dioxide. For germanate glass in presence of TiO_2 (TiGe-Cr), the Cr^{3+} ions are located in the higher crystal field and, thus, the emission of sharp R-line arising from the spin-forbidden ${}^2E \rightarrow {}^4A_2$ transition is more intense. When the Cr^{3+} ions are located in the lower crystal field, broadband emission originating from the spin-allowed ${}^4T_2 \rightarrow {}^4A_2$ transition is dominated (Ge-Cr). There is in a good agreement with the results obtained previously for fluoride-sulfophosphate glasses, which are promising hosts for broadband optical amplification through transition metal activators [39].

3.3. Titanate-Germanate Glasses Doped with Europium Ions

Excitation (Figure 3a) and emission (Figure 3b) spectra, and decay curves (Figure 3c) measured for titanate-germanate glasses doped with europium ions (TiGe-Eu) are presented in Figure 3. The results are compared to glass samples without TiO_2 (Ge-Eu). All changes are also schematized on Figure 3d–f.

The excitation spectrum consists of several bands, which originate from the 7F_0 ground state to the higher-lying 5D_2 , 5D_3 , 5L_6 , 5L_7 , 5G_1 , and 5D_4 excited states of europium ions. The most intense bands are due to ${}^7F_0 \rightarrow {}^5L_6$ (near 390 nm) and ${}^7F_0 \rightarrow {}^5D_2$ (near 460 nm) transitions. The later transition is known as the pure electronic transition (PET). In this spectral region, the phonon sideband (PSB) is also located and associated with the pure electronic transition (PET). The difference between the positions of both PSB and PET bands is well-known as the phonon energy of the host. Our studies indicate that the phonon energy of the glass host is reduced from 790 cm^{-1} (Ge-Eu) to 765 cm^{-1} with the presence of TiO_2 (TiGe-Eu). From phonon sideband measurements [40–42], the electron–phonon

coupling strength g can be also estimated, which is due to the intensity ratio of the PSB ($\int I_{\text{PSB}} d\nu$) to the PET ($\int I_{\text{PET}} d\nu$), respectively. The results are given in Table 2.

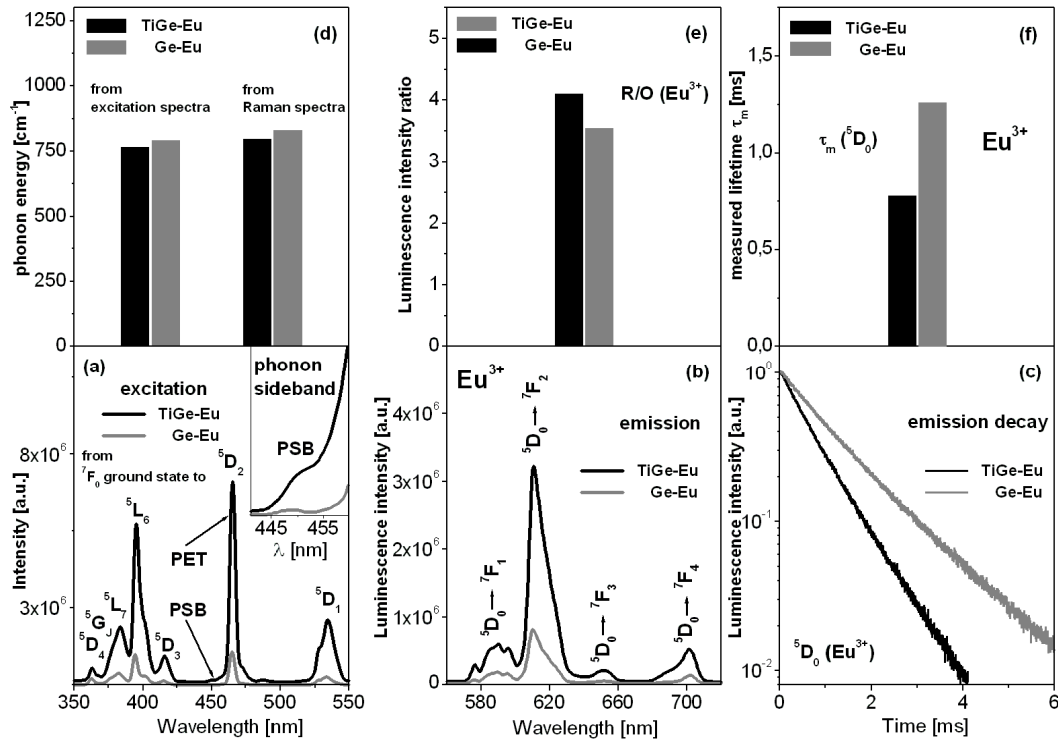


Figure 3. Excitation (a) and emission (b) spectra, and decay curves (c) for titanate–germanate glasses doped with europium ions (TiGe-Eu) and compared to glass samples without TiO₂ (Ge-Eu). All changes are also schematized (d–f).

Table 2. Spectroscopic parameters for europium ions in glasses TiGe-Eu and Ge-Eu.

Spectroscopic Parameter	TiGe-Eu	Ge-Eu
PSB–PET (cm ^{−1})	765	790
Electron–phonon coupling strength g ($\times 10^{-3}$)	1.7	5.2
Non-radiative relaxation rate $W_p(T)/W_0(0)$ (s ^{−1})		
from ⁵ D ₁ state	6.85×10^{-7}	1.37×10^{-5}
from ⁵ D ₂ state	4.87×10^{-10}	3.66×10^{-8}

Finally, the multiphonon relaxation rate $W_p(T)$ depending on the electron–phonon coupling strength and phonon energy of the glass host can be determined as follows $W_p(T) = W_0(0)\exp(-\alpha\Delta E)$, where $W_0(0)$ is the transition probability extrapolated to zero energy gap, ΔE denotes the energy gap between neighboring energy states and the values of ⁵D₁–⁵D₀ and ⁵D₂–⁵D₁ energy gaps of Eu³⁺ ions are equal nearly to 1750 cm^{−1} and 2500 cm^{−1}, respectively. In this relation the α parameter is close to $(\ln(p/g)-1)/h\omega$, where $h\omega$ represents the phonon energy, g —the electron–phonon coupling strength, and p as the phonon number is equal to $\Delta E/h\omega$. In some cases, the multiphonon relaxation rate is given as $W_p(T)/W_0(0)$ [43]. Our spectroscopic calculations presented in Table 2 clearly indicate that the electron–phonon coupling strength and multiphonon relaxation rates from the ⁵D₁ and ⁵D₂ states of europium ions are significantly smaller for glass sample with the presence of titanium dioxide.

Further experimental investigations shown on Figure 3 suggest that titanate–germanate glass demonstrates the efficient reddish-orange emission independently on the excitation wavelengths at 390 nm (⁵L₆ state) or 460 nm (⁵D₂ state) and its intensity is considerably higher in comparison to the

glass sample without titanium dioxide. The emission bands correspond to the electronic transitions originating from the 5D_0 state to the 7F_J ($J = 1-4$) states of europium ions, respectively.

In order to evaluate the glass asymmetry and the strength of bonding (covalent/ionic character) between europium ions and their surroundings, the ratio of integrated band intensity of $^5D_0 \rightarrow ^7F_2$ transition to that of the $^5D_0 \rightarrow ^7F_1$ transition, well-known in literature as red-to-orange factor R/O (Eu^{3+}), was calculated. It is generally accepted that the value of R/O (Eu^{3+}) starts to increase with increasing local asymmetry and covalent bonding. This phenomenon is just observed for our glass sample with the presence of titanium dioxide. For the studied systems, the fluorescence intensity ratio R/O (Eu^{3+}) was changed from 3.54 (Ge-Eu) to 4.10 (TiGe-Eu).

Based on decay curve measurements, the luminescence lifetimes for the 5D_0 state of europium ions were also determined. In general, the multiphonon relaxation rates decrease with decreasing phonon energy of the glass-host and consequently the lifetimes measured for excited states of rare earths are usually enhanced. Completely opposite situation is observed for europium ions, because the energy gap between 5D_0 state and lower-lying 7F_6 state of europium ions is very large. Its value seems to be nearly $12,500 \text{ cm}^{-1}$. In this case, several phonons are needed to bridge energy gap and radiative relaxation is a dominant transition. For low-phonon glass systems containing europium ions, the non-radiative relaxation rate is negligibly small in contrast to the radiative relaxation rate. Thus, the nonradiative relaxation rate can be ignored. In a practice, the radiative relaxation rate represents total relaxation rate. The spectroscopic consequence is reduction of luminescence lifetime (as an inverse of total radiative relaxation rate) for the 5D_0 state of europium ions with decreasing phonon energy of the glass-host. These phenomena were presented and discussed in our previous published work [44]. The analysis of luminescence decay curves for glass samples with the presence and absence of titanium dioxide confirms the hypothesis given above. The measured lifetime τ_m for the 5D_0 state of europium ions is reduced from 1.26 ms (Ge-Eu) to 0.78 ms (TiGe-Eu), when the phonon energy decreases from 790 cm^{-1} to 765 cm^{-1} for glass sample with the presence of TiO_2 . It suggests that the influence of titanium dioxide on spectroscopic parameters of europium ions is significant. The changes of phonon energy, fluorescence intensity ratio R/O, and 5D_0 measured lifetime of Eu^{3+} ions in function of TiO_2 are also schematized in Figure 3d–f.

The effects of TiO_2 on luminescence behavior of germanate glass depend greatly on the kind of active dopants (transition metal or rare earth). Luminescence properties of germanate glasses in the presence of TiO_2 are completely different for europium ions than chromium ions discussed in previous Part 3.2. In particular, the intensities of luminescence bands of the optically active ions are changed drastically, when GeO_2 was substituted by TiO_2 in the glass composition. The intensities of luminescence bands of chromium ions are reduced, whereas the emission band intensities of europium ions increase significantly in the presence of TiO_2 . Compared to the results for similar glass-hosts published recently [45–48], we postulate that our multicomponent titanate-germanate glass doped with Eu^{3+} ions is suitable as red-emitting component for LED applications.

First of all, the significant advantage of our systems is the lower phonon energy of the host in comparison to other oxide glasses such as borate ($\sim 1400 \text{ cm}^{-1}$), phosphate ($\sim 1200 \text{ cm}^{-1}$), and silicate ($\sim 1050 \text{ cm}^{-1}$) systems [49–51]. It is assumed that glasses with low phonon energy are more suitable as host materials for rare earth ions because of less probable non-radiative relaxation process, which may result in a higher lifetime of the excited state. According to experimental results presented in Table 3, the luminescence lifetime for 5D_0 excited state evaluated for glass samples (Ge-Eu and TiGe-Eu) is similar to the values obtained for various germanate systems doped with europium ions [52–60]. However, as has already been discussed for low-phonon glass-hosts containing Eu^{3+} ions, the non-radiative relaxation process can be neglected. Thus, the luminescence lifetime as an inverse of total radiative relaxation rate reduces with decreasing phonon energy of the glass-host. Therefore, the value of lifetime for 5D_0 state in glass sample Ge-Eu (790 cm^{-1}) is longer than the value of lifetime for systems with titanium oxide (765 cm^{-1}), lead oxide (775 cm^{-1}), and bismuth oxide (770 cm^{-1}) [51–53]. Moreover, it was stated that the fluorescence intensity ratio R/O (Eu^{3+}) was

increased from 3.54 (Ge-Eu) to 4.10 (TiGe-Eu) for the glass samples and the value of this spectroscopic parameters is significantly higher than those of lead germanate glasses [52,57] antimony [55] and tellurium [56] oxides-modified germanate systems. The obtained value of the ratio R/O indicates the higher local asymmetry around the Eu^{3+} ions in the glass host. It is worth noting that this factor confirms that the addition of a high concentration of titanium dioxide to the germanate matrix does not prompt the crystallization process, although TiO_2 can be a nucleating agent in glass host. Taking this issue into consideration, further research is needed to determine if a thermally stable and fully amorphous system with relatively high titanium oxide content is a good candidate for optical materials, that may find potential use in photonic devices such as optical fibers and amplifiers.

Table 3. Comparison of spectroscopic parameters of Eu^{3+} -doped germanate glasses.

Glass Composition	R/O	τ_m (ms)	References
Ge-Eu	3.54	1.26	present work
TiGe-Eu	4.10	0.78	present work
PbO-GeO ₂ -Ga ₂ O ₃	3.06	1.11	[52]
Bi ₂ O ₃ -GeO ₂	3.94	1.03	[53]
GeO ₂ -Nb ₂ O ₅ -Li ₂ O	6.50	0.81	[54]
GeO ₂ -Nb ₂ O ₅ -Na ₂ O	9.00	0.76	[54]
GeO ₂ -Ga ₂ O ₃ -BaO-Sb ₂ O ₃	1.94	-	[55]
GeO ₂ -Ga ₂ O ₃ -BaO-TeO ₂	2.49	-	[56]
PbO-GeO ₂	2.86	-	[57]
Sb ₂ O ₃ -GeO ₂ -B ₂ O ₃ -Al ₂ O ₃ -Na ₂ O	1.80	-	[58]
GeO ₂ -B ₂ O ₃ -Al ₂ O ₃ -Lu ₂ O ₃ -Gd ₂ O ₃	-	1.43	[59]
GeO ₂ -PbO	-	1.10	[60]

4. Conclusions

Multicomponent titanate-germanate glasses undoped and doped with transition metal (Cr^{3+}) and rare earths (Eu^{3+}) were prepared and then characterized using various experimental techniques: DSC, XRD, EPR, FT-IR, Raman, and luminescence spectroscopy. X-ray diffraction analysis revealed that all received samples are fully amorphous. Thermal and structural studies indicate that the glass transition temperature increases and thermal stability factor is reduced, whereas the Raman and FT-IR bands are shifted to lower frequency region in the presence of TiO_2 . The EPR spectra show typical signals confirming the presence of Cr^{3+} ions at trivalent state and the octahedral coordination. From the excitation spectra (phonon sideband analysis) of Eu^{3+} , the phonon energy of the glass-host, the electron-phonon coupling strength, and the multiphonon relaxation rate were also determined.

In particular, luminescence spectra have been examined for glass samples, where germanium dioxide was substituted by titanium dioxide as well as the relative molar ratio of two glass-former components is equal to $\text{GeO}_2:\text{TiO}_2 = 1:1$. Near-infrared luminescence spectra of chromium ions show two emission bands near 730 nm and 1030 nm, which correspond to the ${}^4\text{T}_2 \rightarrow {}^4\text{A}_2$ transitions in octahedral and tetrahedral sites, respectively. Further spectral analysis suggests that chromium ions occupy higher crystal-field sites in germanate glass with the presence of titanium dioxide. Visible luminescence spectra of europium ions present characteristic emission bands associated to ${}^5\text{D}_0 \rightarrow {}^7\text{F}_j$ ($j = 1-4$) transitions. The red-to-orange fluorescence intensity ratio R/O and the luminescence lifetime for the ${}^5\text{D}_0$ state of europium were determined. The later parameter, i.e., the measured ${}^5\text{D}_0$ lifetime was reduced from 1.26 ms (Ge-Eu) to 0.78 ms (TiGe-Eu). This behavior is quite well correlated with the phonon energy, which decreases from 790 cm^{-1} to 765 cm^{-1} with the presence of titanium dioxide. The factor R/O was changed from 3.54 (Ge-Eu) to 4.10 (TiGe-Eu) suggesting the increase of local asymmetry and stronger covalent character of bonding between europium ions and their nearest surroundings in glass sample in the presence of TiO_2 .

Our spectroscopic studies clearly indicate that luminescence properties of multicomponent titanate-germanate glasses are completely different for transition metal ions than rare earth ions.

The intensities of emission bands of chromium ions are reduced, whereas the emission band intensities of europium ions increase drastically in the presence of TiO₂. The obtained results demonstrate that titanate-germanate glass doped with Eu³⁺ ions is a promising candidate for red luminescence applications.

Author Contributions: Conceptualization, W.A.P.; methodology, M.K., J.P. (Justyna Polak), E.P., and T.G.; formal analysis, W.A.P. and J.P. (Joanna Pisarska); investigation, M.K., K.K., J.P. (Justyna Polak), E.P., T.G., and J.P. (Joanna Pisarska); writing—original draft preparation, W.A.P.; writing—review and editing, W.A.P.; project administration, W.A.P.; funding acquisition, W.A.P. All authors have read and agreed to the published version of the manuscript.

Funding: This research was funded by National Science Centre (Poland), grant number 2018/31/B/ST8/00166.

Conflicts of Interest: The authors declare no conflict of interest.

References

1. Chen, J.; Wei, C. Formation and structure of titanate glasses. *J. Non-Cryst. Solids* **1986**, *80*, 135–140.
2. Fukushima, T.; Benino, Y.; Fujiwara, T.; Dimitrov, V.; Komatsu, T. Electronic polarizability and crystallization of K₂O–TiO₂–GeO₂ glasses with high TiO₂ contents. *J. Solid State Chem.* **2006**, *179*, 3949–3957. [[CrossRef](#)]
3. Masai, H.; Fujiwara, T.; Benino, Y.; Komatsu, T. Large second-order optical nonlinearity in 30BaO–15TiO₂–55GeO₂ surface crystallized glass with strong orientation. *J. Appl. Phys.* **2006**, *100*, 023526. [[CrossRef](#)]
4. Toloman, D.; Suciu, R.; Leostean, C.; Regos, A.; Ardelean, I. The influence of TiO₂ concentration in some calcium-phosphate glasses. *Physica B* **2014**, *438*, 84–87. [[CrossRef](#)]
5. Kirchhof, J.; Unger, S.; Dellith, J.; Scheffel, A. Diffusion in binary TiO₂–SiO₂ glasses. *Opt. Mater. Express* **2014**, *4*, 672–680. [[CrossRef](#)]
6. Slavov, S.S.; Dimitriev, Y.B. Glass formation in the system Bi₂O₃–TiO₂–SiO₂. *J. Chem. Technol. Metall.* **2016**, *51*, 536–546.
7. ElBatal, F.H.; Marzouk, M.A.; ElBatal, H.A. Optical and crystallization studies of titanium dioxide doped sodium and potassium silicate glasses. *J. Mol. Struct.* **2016**, *1121*, 54–59. [[CrossRef](#)]
8. Freschi, C.D.; Gouveia, J.T.; Marcondes, L.; Ferrari, J.L.; Cassanjes, F.C.; Poirier, G. Crystallization of anatase TiO₂ in niobium potassium phosphate glasses. *Mater. Res.* **2017**, *20*, 502–508. [[CrossRef](#)]
9. Pisarska, J.; Kowal, M.; Kochanowicz, M.; Zmojda, J.; Dorosz, J.; Dorosz, D.; Pisarski, W.A. Influence of BaF₂ and activator concentration on broadband near-infrared luminescence of Pr³⁺ ions in gallo-germanate glasses. *Opt. Express* **2016**, *24*, 2427–2435. [[CrossRef](#)]
10. Walas, M.; Lewandowski, T.; Synak, A.; Łapiński, M.; Sadowski, W.; Kościelska, B. Eu³⁺ doped tellurite glass ceramics containing SrF₂ nanocrystals: Preparation, structure and luminescence properties. *J. Alloys Compd.* **2017**, *696*, 619–626. [[CrossRef](#)]
11. Pisarska, J.; Sołtys, M.; Górny, A.; Kochanowicz, M.; Zmojda, J.; Dorosz, J.; Dorosz, D.; Sitarz, M.; Pisarski, W.A. Rare earth-doped barium gallo-germanate glasses and their near-infrared luminescence properties. *Spectrochim. Acta A* **2018**, *201*, 362–366. [[CrossRef](#)] [[PubMed](#)]
12. Zur, L.; Janek, J.; Sołtys, M.; Pisarska, J.; Pisarski, W.A. Effect of BaF₂ content on luminescence of rare-earth ions in borate and germanate glasses. *J. Am. Ceram. Soc.* **2016**, *99*, 2009–2016. [[CrossRef](#)]
13. Upendra Kumar, K.; Prathyusha, V.A.; Babu, P.; Jayasankar, C.K.; Joshi, A.S.; Speghini, A.; Bettinelli, M. Fluorescence properties of Nd³⁺-doped tellurite glasses. *Spectrochim. Acta A* **2007**, *67*, 702–708. [[CrossRef](#)] [[PubMed](#)]
14. Jaba, N.; Ben Mansour, H.; Kanoun, A.; Brenier, A.; Champagnon, B. Spectral broadening and luminescence quenching of 1.53 μm emission in Er³⁺-doped zinc tellurite glass. *J. Lumin.* **2009**, *129*, 270–276. [[CrossRef](#)]
15. Ratnakaram, Y.C.A.; Balakrishna, A.; Rajesh, D. Effect of modifier oxides on absorption and emission properties of Eu³⁺ doped different lithium fluoroborate glass matrices. *Physica B* **2012**, *407*, 4303–4307. [[CrossRef](#)]
16. O’Shaughnessy, C.; Henderson, G.S.; Nesbitt, H.W.; Bancroft, G.M.; Neuville, D.R. The influence of modifier cations on the Raman stretching modes of Qⁿ species in alkali silicate glasses. *J. Am. Ceram. Soc.* **2020**, *103*, 3991–4001. [[CrossRef](#)]

17. Yusub, S.; Rajyasree, C.; Ramesh Babu, A.; Vinaya Teja, P.M.; Krishna Rao, D. Influence of alkaline earth oxides (R = Ca, Sr and Ba) on spectroscopic and dielectric studies of iron doped RO–Na₂O–B₂O₃ glasses. *J. Non-Cryst. Solids* **2013**, *364*, 62–68. [[CrossRef](#)]
18. Janek, J.; Sołtys, M.; Żur, L.; Pietrasik, E.; Pisarska, J.; Pisarski, W.A. Luminescence investigations of rare earth doped lead-free borate glasses modified by MO (M = Ca, Sr, Ba). *Mater. Chem. Phys.* **2016**, *180*, 237–243. [[CrossRef](#)]
19. Sołtys, M.; Żur, L.; Pisarska, J.; Goryczka, T.; Pisarski, W.A. Selective oxide modifiers M₂O₃ (M = Al, Ga) as crystallizing agents in Er³⁺-doped lead phosphate glass host. *Ceram. Int.* **2015**, *41*, 4334–4339. [[CrossRef](#)]
20. Pisarski, W.A.; Pisarska, J.; Żur, L.; Goryczka, T. Structural and optical aspects for Eu³⁺ and Dy³⁺ ions in heavy metal glasses based on PbO–Ga₂O₃–XO₂ (X = Te, Ge, Si). *Opt. Mater.* **2013**, *35*, 1051–1056. [[CrossRef](#)]
21. Marcondes, L.M.; Maestri, S.; Sousa, B.; Goncalves, R.R.; Cassanjes, F.C.; Poirier, G.Y. High niobium oxide content in germanate glasses: Thermal, structural, and optical properties. *J. Am. Ceram. Soc.* **2018**, *101*, 220–230. [[CrossRef](#)]
22. Żur, L.; Janek, J.; Sołtys, M.; Goryczka, T.; Pisarska, J.; Pisarski, W.A. Structural and optical investigations of rare earth doped lead-free germanate glasses modified by MO and MF₂ (M = Ca, Sr, Ba). *J. Non-Cryst. Solids* **2016**, *431*, 145–149. [[CrossRef](#)]
23. Żmojda, J.; Kochanowicz, M.; Miluski, P.; Golonko, P.; Baranowska, A.; Ragiń, T.; Dorosz, J.; Kuwik, M.; Pisarski, W.A.; Pisarska, J.; et al. Luminescent studies on germanate glasses doped with europium ions for photonic applications. *Materials* **2020**, *13*, 2817. [[CrossRef](#)] [[PubMed](#)]
24. Peng, Y.-P.; Yuan, X.; Zhang, J.; Zhang, L. The effect of La₂O₃ in Tm³⁺-doped germanate-tellurite glasses for ~2 μm emission. *Sci. Rep.* **2014**, *4*, 5256. [[CrossRef](#)]
25. Ragiń, T.; Baranowska, A.; Kochanowicz, M.; Zmojda, J.; Miluski, P.; Dorosz, D. Study of mid-infrared emission and structural properties of heavy metal oxide glass and optical fibre co-doped with Ho³⁺/Yb³⁺ ions. *Materials* **2019**, *12*, 1238. [[CrossRef](#)]
26. Wei, T.; Chen, F.; Tian, Y.; Xu, S. Efficient 2.7 μm emission and energy transfer mechanism in Er³⁺ doped Y₂O₃ and Nb₂O₅ modified germanate glasses. *J. Quant. Spectrosc. Radiat.* **2014**, *133*, 663–669. [[CrossRef](#)]
27. de Mello, L.B.; Sigoli, F.A.; Mazali, I.O. Structural and optical properties of erbium and ytterbium codoped germanoniobophosphate glasses. *J. Am. Ceram. Soc.* **2014**, *97*, 2462–2470. [[CrossRef](#)]
28. Pisarski, W.A.; Goryczka, T.; Wodecka-Duś, B.; Płońska, M.; Pisarska, J. Structure and properties of rare earth-doped lead borate glasses. *Mater. Sci. Eng. B* **2005**, *122*, 94–99. [[CrossRef](#)]
29. Grujić, S.; Blagojević, N.; Tošić, M.; Živanović, V.; Božović, B. The effect of TiO₂ on the structure and devitrification behavior of potassium titanium germanate glass. *J. Therm. Anal. Cal.* **2006**, *83*, 463–466. [[CrossRef](#)]
30. Guerineau, T.; Strutynski, C.; Skopak, T.; Morency, S.; Hanafi, A.; Cazavara, F.; Ledemi, Y.; Danto, S.; Cardinal, T.; Messaddeq, Y.; et al. Extended germano-gallate fiber drawing domain: From germanates to gallates optical fibers. *Opt. Mater. Express* **2019**, *9*, 2437–2445. [[CrossRef](#)]
31. Kamitsos, E.I.; Yiannopoulos, Y.D.; Karakassides, M.A.; Chryssikos, G.D.; Jain, H. Raman and infrared structural investigation of xRb₂O-(1-x)GeO₂ glasses. *J. Phys. Chem.* **1996**, *100*, 11755–11765. [[CrossRef](#)]
32. Lu, M.; Wang, F.; Liao, Q.; Chen, K.; Qin, J.; Pan, S. FTIR spectra and thermal properties of TiO₂-doped iron phosphate glasses. *J. Mol. Struct.* **2015**, *1081*, 187–192. [[CrossRef](#)]
33. Narendrudu, T.; Suresh, S.; Chinna Ram, G.; Veeraiyah, N.; Krishna Rao, D. Spectroscopic and structural properties of Cr³⁺ ions in lead niobium germanosilicate glasses. *J. Lumin.* **2017**, *183*, 17–25. [[CrossRef](#)]
34. De Vicente, F.S.; Santos, F.A.; Simões, B.S.; Dias, S.T.; Siu Li, M. EPR, optical absorption and luminescence studies of Cr³⁺-doped antimony phosphate glasses. *Opt. Mater.* **2014**, *38*, 119–125. [[CrossRef](#)]
35. Murali, A.; Rao, J.L. Electron paramagnetic resonance and optical absorption spectra of Cr³⁺ ions in fluorophosphate glasses. *J. Phys. Condens. Matter* **1999**, *11*, 1321–1331. [[CrossRef](#)]
36. Pisarska, J.; Kuwik, M.; Górný, A.; Dorosz, J.; Kochanowicz, M.; Zmojda, J.; Sitarz, M.; Dorosz, D.; Pisarski, W.A. Influence of transition metal ion concentration on near-infrared emission of Ho³⁺ in barium gallo-germanate glasses. *J. Alloys Compd.* **2019**, *793*, 107–114. [[CrossRef](#)]
37. Li, Y.; Ye, S.; Zhang, Q. Ultra-broadband near-infrared luminescence of ordered–disordered multi-sited Cr³⁺ in La₃Ga_{5.5}Nb_{0.5}O₁₄:Cr³⁺. *J. Mater. Chem. C* **2014**, *2*, 4636–4641. [[CrossRef](#)]

38. Pisarski, W.A.; Pisarska, J.; Dominiak-Dzik, G.; Ryba-Romanowski, W. Transition metal (Cr^{3+}) and rare earth (Eu^{3+} , Dy^{3+}) ions used as a spectroscopic probe in compositional-dependent lead borate glasses. *J. Alloys Compd.* **2009**, *484*, 45–49. [[CrossRef](#)]
39. Wang, W.C.; Le, Q.H.; Zhang, Q.Y.; Wondraczek, L. Fluoride-sulfophosphate glasses as hosts for broadband optical amplification through transition metal activators. *J. Mater. Chem. C* **2017**, *5*, 7969–7976. [[CrossRef](#)]
40. Ramachari, D.; Rama Moorthy, L.; Jayasankar, C.K. Phonon sideband spectrum and vibrational analysis of Eu^{3+} -doped niobium oxyfluorosilicate glass. *J. Lumin.* **2013**, *143*, 674–679. [[CrossRef](#)]
41. Manasa, P.; Jayasankar, C.K. Luminescence and phonon side band analysis of Eu^{3+} -doped lead fluorosilicate glasses. *Opt. Mater.* **2016**, *62*, 139–145. [[CrossRef](#)]
42. Rajesh, M.; Reddy, G.R.; Sushma, N.J.; Devarajulu, G.; Deva Prasad Raju, B. Phonon sideband analysis, structural and spectroscopic properties of Eu^{3+} ions embedded $\text{SiO}_2\text{-B}_2\text{O}_3\text{-CaF}_2\text{-NaF-Na}_2\text{O}$ glasses. *Opt. Mater.* **2020**, *107*, 110038. [[CrossRef](#)]
43. Vijaya Prakash, G.; Jagannathan, R. Fluorescence properties of Eu^{3+} doped lead bearing fluoro-chloro phosphate glasses. *Spectrochim. Acta A* **1999**, *55*, 1799–1808. [[CrossRef](#)]
44. Pisarski, W.A.; Zur, L.; Kowal, M.; Pisarska, J. Enhancement and quenching photoluminescence effects for rare earth - doped lead bismuth gallate glasses. *J. Alloys Compd.* **2015**, *651*, 565–570. [[CrossRef](#)]
45. Aryal, P.; Kim, H.J.; Khan, A.; Saha, S.; Kang, S.J.; Kothan, S.; Yamsuk, Y.; Kaewkhao, J. Development of Eu^{3+} -doped phosphate glass for red luminescent solid-state optical devices. *J. Lumin.* **2020**, *227*, 117564. [[CrossRef](#)]
46. Roy, J.S.; Messaddeq, Y. Photoluminescence study of Eu^{3+} doped zinc-tungsten-antimonite glasses for red LED applications. *J. Lumin.* **2020**, *228*, 117608. [[CrossRef](#)]
47. Lakshminarayana, G.; Wagh, A.; Kamath, S.D.; Dahshan, A.; Hegazy, H.H.; Marzec, M.; Kityk, I.V.; Lee, D.-E.; Yoon, J.; Park, T. Eu^{3+} -doped fluoro-telluroborate glasses as red-emitting components for W-LEDs application. *Opt. Mater.* **2020**, *99*, 109555. [[CrossRef](#)]
48. Maity, A.; Jana, S.; Ghosh, S.; Sharma, S. Spectroscopic investigation on europium (Eu^{3+}) doped strontium zinc lead phosphate glasses with varied ZnO and PbO compositions. *J. Non-Cryst. Solids* **2020**, *550*, 120322. [[CrossRef](#)]
49. Vázquez, G.V.; Muñoz, H.G.; Camarillo, I.; Falcony, C.; Caldiño, U.; Lira, A. Spectroscopic analysis of a novel Nd^{3+} -activated barium borate glass for broadband laser amplification. *Opt. Mater.* **2015**, *46*, 97–103. [[CrossRef](#)]
50. Mazurak, Z.; Bodył, S.; Lisiecki, R.; Gabryś-Pisarska, J.; Czaja, M. Optical properties of Pr^{3+} , Sm^{3+} and Er^{3+} doped $\text{P}_2\text{O}_5\text{-CaO-SrO-BaO}$ phosphate glass. *Opt. Mater.* **2010**, *32*, 547–553. [[CrossRef](#)]
51. Pisarska, J.; Zur, L.; Pisarski, W.A. Optical spectroscopy of Dy^{3+} ions in heavy metal lead-based glasses and glass-ceramics. *J. Mol. Struct.* **2011**, *993*, 160–166. [[CrossRef](#)]
52. Zur, L. Structural and luminescence properties of Eu^{3+} , Dy^{3+} and Tb^{3+} ions in lead germanate glasses obtained by conventional high-temperature melt-quenching technique. *J. Mol. Struct.* **2013**, *1041*, 50–54. [[CrossRef](#)]
53. Gökçe, M. Development of Eu^{3+} doped bismuth germanate glasses for red laser applications. *J. Non-Cryst. Solids* **2019**, *505*, 272–278. [[CrossRef](#)]
54. Guedes, L.F.N.; Marcondes, L.M.; Evangelista, R.O.; Batista, G.; Mendoza, V.G.; Cassanjes, F.C.; Poirier, G.Y. Effect of alkaline modifiers on the structural, optical and crystallization properties of niobium germanate glasses and glass-ceramics. *Opt. Mater.* **2020**, *105*, 109866. [[CrossRef](#)]
55. Szal, R.; Zmojda, J.; Kochanowicz, M.; Miluski, P.; Dorosz, J.; Leśniak, M.; Jeleń, P.; Starzyk, B.; Sitarz, M.; Kuwik, M.; et al. Spectroscopic properties of antimony modified germanate glass doped with Eu^{3+} ions. *Ceram. Int.* **2019**, *45*, 24811–24817. [[CrossRef](#)]
56. Jadach, R.; Zmojda, J.; Kochanowicz, M.; Miluski, P.; Leśniak, M.; Sołtys, M.; Pisarska, J.; Pisarski, W.A.; Lukowiak, A.; Sitarz, M.; et al. Spectroscopic properties of rare earth doped germanate glasses. *Proc. SPIE* **2018**, *10683*, 1068316.
57. Wachtler, M.; Speghini, A.; Gatterer, K.; Fritzer, H.P.; Ajò, D.; Bettinelli, M. Optical Properties of Rare-Earth Ions in Lead Germanate Glasses. *J. Am. Ceram. Soc.* **1998**, *81*, 2045–2052. [[CrossRef](#)]
58. Zmojda, J.; Kochanowicz, M.; Miluski, P.; Baranowska, A.; Pisarski, W.A.; Pisarska, J.; Jadach, R.; Sitarz, M.; Dorosz, D. Structural and optical properties of antimony-germanate-borate glass and glass-fiber co-doped Eu^{3+} and Ag nanoparticles. *Spectrochim. Acta A* **2018**, *201*, 1–7. [[CrossRef](#)]

59. Wang, X.; Huang, L.; Zhao, S.; Xu, S. Eu^{3+} doped heavy germanate scintillating glasses. *J. Lumin.* **2018**, *196*, 256–258. [[CrossRef](#)]
60. Bensalem, C.; Mortier, M.; Vivien, D.; Diaf, M. Thermal and optical investigation of EuF_3 -doped lead fluorogermanate glasses. *J. Non-Cryst. Solids* **2010**, *356*, 56–64. [[CrossRef](#)]



© 2020 by the authors. Licensee MDPI, Basel, Switzerland. This article is an open access article distributed under the terms and conditions of the Creative Commons Attribution (CC BY) license (<http://creativecommons.org/licenses/by/4.0/>).